Interaction of a vortex ring with a piston vortex

J. J. Allen and B. Auvity [*]

Department of Mechanical and Aerospace Engineering

Princeton University, Princeton, NJ, 08540

Recent studies on vortex ring generation, e.g. Rosenfeld *et al.* (1998), have highlighted the subtle effect on generation geometry on the final properties of rings. Experimental generation of vortex rings often involves moving a piston through a tube, resulting in a vortex ring being generated at the tube exit. A generation geometry that has been cited as a standard consists of the tube exit mounted flush with a wall with the piston stroke ending at the tube exit, Glezer (1988). We employ this geometry to investigate the effect of the vortex that forms in front of the advancing piston (*piston vortex*) on the primary vortex ring that is formed at the tube exit. It is shown that when the piston finishes its stroke flush with the wall, and hence forms an uninterrupted plane, the piston vortex is convected through the primary ring and then ingested into the primary vortex. The ingestion of the piston vortex results in an increased ring impulse and an altered trajectory, when compared to the case when the piston motion is finished inside the tube. As the Reynolds number of the experiments, based on the piston speed and piston diameter, is the order of three thousand, transition to turbulence is observed during the self-induced translation phase of the ring motion. Compared to the case when the piston is stopped inside the tube, the vortex ring which has ingested the piston vortex transitions

[(*)] Present address: Laboratoire d'Etudes Aérodynamiques/Centre d'Etudes Aérodynamiques et Thermiques - 43, rue de l'aérodrome - 86036 Poitiers Cedex – FRANCE.

to turbulence at a significantly reduced distance from the orifice exit and suggests the transition map suggested by Glezer (1988) is somewhat under question. A secondary instability characterized by vorticity filaments with components in the axial and radial direction, was observed forming on the piston vortex. The structure of the instability appears to be similar to the streamwise vortex filaments that form in the braid regions of shear layers This instability was subsequently ingested into the primary ring during the translation phase and may act to accelerate the growth of the Tsai-Widnall instability. It is suggested that the origin of the instability is Görtler in nature and the result of unsteady wall jet nature of the boundary layer separating on the piston face.

1. Introduction

The dynamics of vortex rings is a subject that has long fascinated researchers in fluid dynamics. Experimental research in this field is undergoing somewhat of a renaissance with the use of synthetic jets, which are essentially a stream of vortex rings, for flow control. Comprehensive reviews of the behavior of vortex rings are provided by Shariff & Leonard (1992) and Lim & Nickels (1995). Experimental generation of vortex rings often involves moving a piston through a tube, resulting in a vortex ring being generated at the tube exit. The development of a vortex ring typically passes through a number of stages of development, i.e. the formation phase, the laminar phase, the transitional phase and finally, the turbulent phase. Lim & Nickels (1995) note that whether the ring passes through all four phases is dependent on the initial conditions

during the formation phase. During the formation phase, the early transient development of a vortex was described using similarity arguments, Pullin (1978). Experiments and computations have had varied success in identifying a period of self-similar behavior, Didden (1979), Pullin & Perry (1980), Nitsche & Krasny (1994), Heeg & Riley (1997), James & Madnia (1996). The discrepancy from similarity theory has been explained in terms of a number of effects, ranging from the self-induced effect, secondary vorticity and viscous entrainment by the ring. For short non-dimensional stroke length L/D, where L is the distance moved by the piston and D is the piston diameter, the end of the formation phase is determined by the cessation of the piston motion. It corresponds to the point of transition from a growing vortex ring of increasing strength to where the ring begins to convect as a result of its self-induced velocity. This point is marked by a contraction of the ring diameter to reach a stable diameter, see Didden (1979) and Gharib & Weigand (1998). Didden (1979) states that the final non-dimensional diameter of the vortex is a function solely of L/D. It is also slightly dependent on the geometry of the generator, Lim & Nickels (1995). For fixed L/D, the vortex trajectory, and hence the final ring diameter, are almost independent on the Reynolds number for a wide range of Reynolds number up to 70000, see Maxworthy (1977), Reynolds number based on the piston speed and the piston diameter. The cause of the diameter reduction is an open question. It is suggested, Didden (1979), Sheffield (1977), that the contraction is partly due to the effect of the image vortex in the wall and partly due to the *stopping vortex*. When the piston is brought to an abrupt halt, the primary vortex induces a separation at the corner of the generation geometry resulting in the formation of a vortex. This stopping vortex has been observed in a range of studies, e.g. Pullin & Perry (1980) and

Weigand & Gharib (1997). The significance of the effect of the stopping vortex on the trajectory of the primary vortex is also an open question. For example Didden (1979) believed its effect to be weak and Heeg & Riley (1997) believed its effect to be strong. James & Madnia (1996) studied the ring produced at a nozzle and orifice. Their computations show a difference in final ring diameter between the two generation apparatus, for a given L/D. They attributed this difference to the lack of a wall effect for the nozzle as the stopping vortex was present in both cases. Another reason for this difference could be the ingestion into the ring of the secondary vorticity generated on the walls close to the orifice. Besides, if the effects of image are important it would be expected that the nature of the generation geometry would be important. The magnitude of L/D plays an important role in determining the resulting motion. If L/D~0.1 Sheffield (1977) showed the effects of the vortex image and stopping vortex are strong relative to the self-induced effect, and the potential exists for the ring to propagate back into the tube. For L/D of the order $0.5 \rightarrow 4.5$, the ring will convect away form the orifice under its self-induced field. The vortex will not continue to grow as a discrete structure for increasing L/D and eventually the flow transitions to a jet, as mentioned by Saffman (1978). A criterion for the maximum piston displacement in relation to the vortex diameter that results in a discrete vortex, has been proposed by Gharib *et al.* (1998) as being L/D~$3.6 \rightarrow 4.5$. A physical argument for this limiting value of L/D was suggested as "*the apparatus is no longer able to deliver energy at a rate compatible with the requirement that a steady translating vortex ring have maximum energy with respect to impulse-preserving iso-vortical perturbations*". This result has provoked a considerable amount of interest and resulted in a number of publications examining formation

numbers. A recent paper by Linden & Turner (2001) equates the circulation, impulse and energy provided to the ring during generation to the properties of a particular class of rings with finite cores described by Norbury (1973). This formulation leads to the important result that the resultant ring diameter is essentially a function of the impulse, kinetic energy and circulation delivered to the ring during the formation phase. This suggests that the effects of image and stopping vortex are small, in as much as generator effects act to modify these invariants and resultant vorticity distribution.

As the vortex convects away from the generating orifice, if the Reynolds number based on piston speed and diameter exceeds 600, then the potential exists for it to develop a wavy structure. This is a precursor to breakdown to turbulence. An inviscid model for the appearance of azimuthal waves on the ring is described by Widnall & Tsai (1977). The wave number of the most unstable waves was found to be independent of Reynolds number. Experiments however show a variation in the number of waves on a ring, e.g. Leiss & Didden (1978). The reason for this was explained by Saffman (1978) who determined that shape of the vorticity distribution within the core can affect the number of waves that are formed on the ring. Studies of the behavior of transitional to turbulent rings are relatively limited. Maxworthy (1974) observed the appearance of the Widnall instability prior to breakdown. Glezer (1988) notes that the transition to turbulence is preceded by the formation of a secondary instability on the primary vortex which appears similar in form to the secondary instability on a plane mixing layer, e.g. Bernal & Roshko (1986). Glezer (1988) noted the existence of Kelvin-Helmholtz instabilities on the vortex sheet connecting the vortex core to the generation orifice. He suggested that the ingestion of these instabilities into the vortex ring may accelerate the onset of turbulence. Glezer &

Coles (1990) argue that these structures have a significant global effect in terms of acting to entrain fluid into the ring. The photographs of Maxworthy (1974) also show evidence of Kelvin-Helmholtz instabilities on the shear layer at a Reynolds number, Re_D, based on piston speed and piston diameter of the order ten thousand. Lim (1997) conducted detailed experiments to examine the interaction of the shear layer instability with the vortex core concluded that ingestion of shear layer instability hastened the transition to turbulence. Glezer (1988) suggested a generation geometry that consists of a tube that exits into a plane wall, with the piston finishing flush with the wall at the end of the generation process, forming an uninterrupted plane. This geometry has the obvious effect of removing the singularity that exists at the orifice edge of the tube exit when the piston motion stops (stopping vortex). This experiment raises the interesting question as to what happens to the *piston vortex* that has been formed in front of the advancing piston. Experiments of Tabaczynski *et al.* (1970), Hughes & Gerrard (1971) and Allen & Chong (2000) have shown that for Reynolds number greater than four hundred, based on piston speed and diameter, a vortex forms in front of the piston as it advances through the cylinder. The mechanism for this vortex formation is the removal of the boundary layer from the cylinder wall in front of the advancing piston. Lim (2000) and Cater *et al*. (1998) suggest from preliminary flow visualization studies that for an L/D=3 there is an interaction between the primary ring and the piston vortex via vortex leapfrogging with the effect of hastening a transition to turbulence. Allen *et al.* (2000) used dye visualization to show the interaction of the piston vortex and primary ring for L/D=2 and their vorticity field measurements showed the presence of the piston vortex and its ingestion into the primary core.

Based on this short review, a number of questions need to be addressed when using a generation geometry of the form proposed by Glezer (1988).

- What is the effect of the stopping vortex? Can it be quantified using similar generation condition (same non-dimensional stroke length and piston speed) but different stopping geometry? , i.e. the piston stops flush with the wall or inside the tube.
- What is the effect of the piston vortex on the primary ring and what is the nature of the interaction between them?
- Does the interaction changes the transition process of the ring? Does the piston vortex trigger any particular type of instability on the primary ring? Does the universal transition map of Glezer (1988) needs re-examination?

2. Experimental apparatus

A schematic of the vortex ring generator is shown in figure 1(a). The diameter of the piston D is 50.8 mm and the lead screw drives the piston up to a maximum speed, U_p, equal to 66.3 mm/s. The orifice plate exits into a 100x50x50cm tank and the maximum piston stroke is 4D. The piston was driven with one velocity characteristic in these experiments, shown in figure 1(b). The average velocity of the piston during its stroke is defined as $\overline{U}_p = 1/T \int_0^T U_p(t)dt$ where T is the duration of the piston motion. The length of the slug ejected from the tube can be described as $L = \int_0^T U_p(t)dt = \overline{U}_p T$ which is also the piston stroke. If the velocity profile at the orifice exit is assumed to be uniform spatially,

then an approximation for the circulation delivered to the ring during generation is expressed as $\Gamma = 1/2 \int_0^T U_P^2(t)dt$.

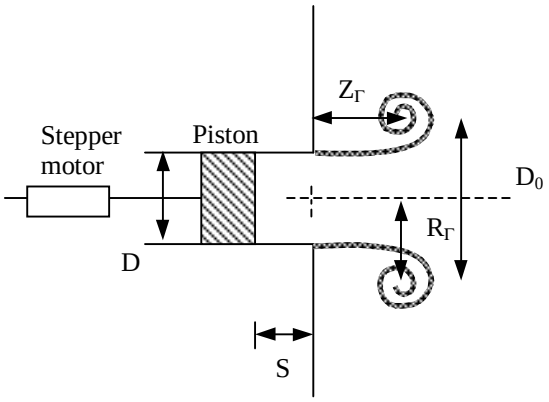

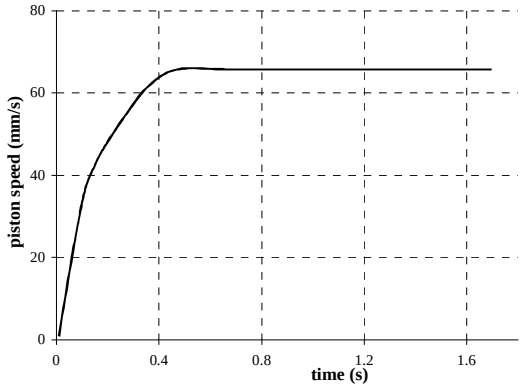

(a) (b)

Figure 1(a) Schematic of the experimental apparatus and (b) piston velocity characteristic.

This model for the ring circulation is often referred to as the "slug" model, see Shariff & Leonard (1992) and Lim & Nickels (1995) for details. Glezer (1988) pointed out that although this model cannot accurately predict the total circulation in the flow, it can be used for comparing the relative circulation of vortex rings formed from the same generator. Didden (1979) showed that this model for the circulation underestimates the strength of the ring by as much as 25%. The reasons are related to the non-uniform (spatial) nature of the velocity profile at the orifice exit during ring production and the ingestion of secondary vorticity. A program factor, *P*, that can be introduced to describe the effect of time variation of the piston velocity can be expressed as

$P = \int_0^1 U_p^2 / \overline{U}_p^2 d(t/T)$, see Glezer(1988). Using this expression an approximation for the circulation of the ring can expressed as $\Gamma = PL^2 / 2T$. An invariant of the vortex motion is the impulse that is delivered to the fluid via non-conservative forces. The ring impulse, expressed in terms of the resulting vorticity field Ω, is $I = 1/2\rho \int r \times \mathbf{\Omega} \delta V$. Using the "slug" model, the impulse delivered to the ring can be approximated as $I = \rho D^2 \pi / 4 \int_0^T U_p^2(t) dt = P\overline{U}_p L \rho \pi D^2 / 4$. A Reynolds number that reflects the approximate impulse of the ring can be defined as $\boldsymbol{Re}_\Gamma = P\overline{U}_p L / \upsilon = 2\Gamma / \upsilon$. Details of generation conditions for the current experiment are listed in table 1. A Reynolds number whose length scale is based on the piston diameter is Re_D.

L/D	U_p mm/sec	$\overline{U}_p$ mm/sec	P	Re_Γ
1.0	66.3	56.3	1.16	3317
2.0	66.3	61.8	1.06	6530
3.0	66.3	62.6	1.05	10030
4.0	66.3	63.5	1.0	13390

Table 1. Experimental conditions

3. Visualization of interaction of piston vortex with primary ring

Fluorescent dye was introduced through the piston via diametrically opposed 0.5mm holes, placed close to the piston/cylinder junction in order to visualize the piston vortex. Dye was also introduced through the tube at the junction of the tube with the wall to visualize the primary vortex. Laser cross sections were taken in a plane through the axis of symmetry of the tube to record the interaction of the piston vortex with the primary ring. For the first set of flow visualization experiments, L/D was varied from $1 \rightarrow 4$ and the piston was finished flush with the wall to determine over what range of L/D an interaction occurred. The images shown in figure 2 are of the piston finishing flush with the wall after moving L/D =1, 2 and 4 respectively. The non-dimensional time t^* shown in figure 2 is defined as $t^*=tU_p/D$. $t^*=0$ corresponds to the start of piston motion.

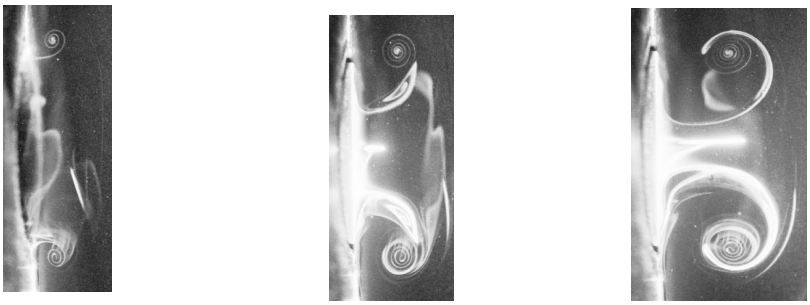

t^*=0.7 t*=1.1 t*=1.8

(a)

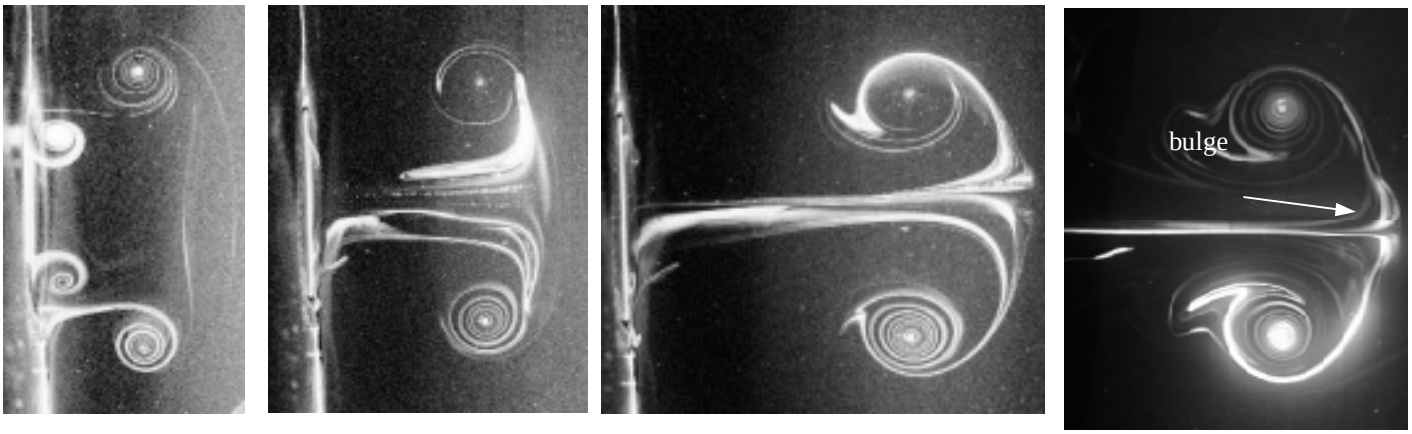

t*=2.1 t*=3.3 t*=4.4 t^*=5.2

(b)

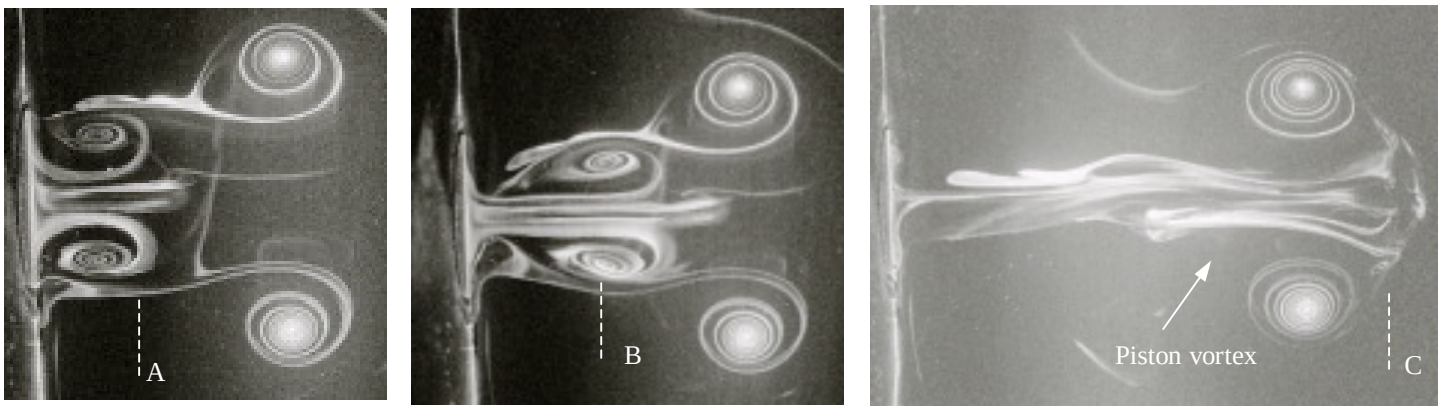

t*=3.9 t*=4.8 t*=6.52

(c)

Figure 2. Piston vortex and vortex ring interaction for (a) Re_Γ=3317, L/D=1 (b) Re_Γ=6530, L/D=2 (c) Re_Γ=13390, L/D=4

In all cases the piston vortex is completely ingested into the primary ring. The flow visualization sequences in figure 2 show that the piston vortex convects rapidly through the core of the main ring toward the forward stagnation point of the primary ring as a result of the induction of the primary ring. When the piston vortex reaches the forward stagnation point it is then rapidly stretched around the outside of the ring, see figure 2(b). Close to the forward stagnation point of the primary vortex some of the dye from the piston vortex appears to be drawn through the ring, forming a characteristic "bulge" in front of the ring, figures 2(b) t*=5.2 and 2(c) t*=6.52. The photographs of Glezer (1988), figure 9(b) and 9(c) show a bulging near the head of the primary ring. This feature of the flow visualizations is a result of the ingestion of the piston vortex. When the piston was stopped inside the tube, no bulge was present. The images in figure 2 show a distinctly tighter spiral shape for the primary ring core than the piston vortex. This would indicate the presence of stronger vorticity in the primary ring core, compared to the piston vortex (this result is confirmed by the Particle Image Velocimetry, PIV , measurements

presented in section 6). Detailed PIV experiments of Allen & Chong (2000) have shown that the piston vortex circulation, Γ_{Piston_vortex}, is of the order 22% the "slug" flow model of the primary vortex, i.e. $\Gamma_{Piston\_vortex}=0.11Re_{\Gamma}$. This result is independent of D.

In terms of vortex sheets, the piston vortex and primary vortex represent separate ends of a layer of vorticity. Connecting these two structures is the layer of vorticity on the cylinder surface. As the piston progresses through the tube this layer is both ejected from the orifice (primary vortex) and scraped up in front of the advancing piston (piston vortex). The relationship between the two structures is shown schematically in figure 3(a). The connecting shear layer between the two structures is clearly evident in the photograph in figure 3(b), which shows the pair at the instant the piston motion has ceased and the piston vortex is being ejected from the tube.

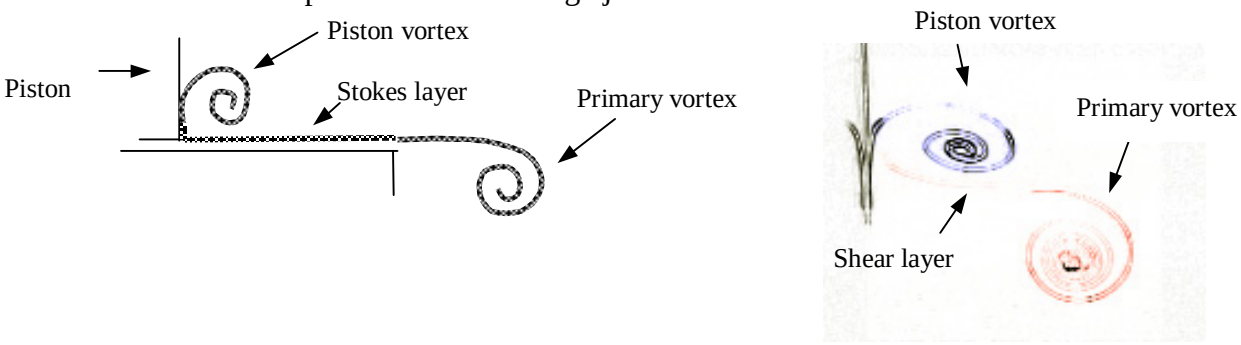

Figure 3. (a) Schematic of the relationship between piston vortex and primary vortex and (b) flow visualization experimental result for Re_{Γ}=6530, L/D=2, t^*=2.17

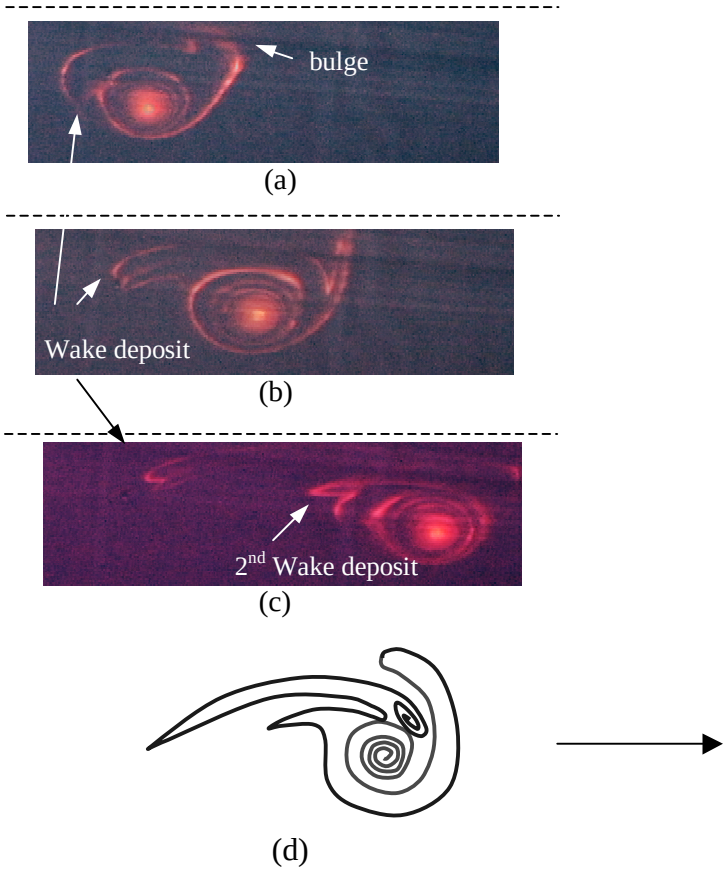

Figure 4. Re_Γ=10030, L/D=3.0 (a) t^*= 6.5 (b) t^*=7.8 (c) t*=10.3 (d) Interpretation of vortex sheet folding.

Figure 4(a-c) show visualizations of a section of the ring at large t^*, during the steady translation phase. In figure 4(a) and (b) the characteristic bulge leading the ring can be seen along with the dye from the piston face being deposited into the ring wake. In figure 4(c) the bulge in figure 4(a) has been convected around the outside ring and a second discrete deposit of dye appears to have been made into the wake. The suggested folding and stretching pattern of the vortex sheets required to produce this detrainment is illustrated in figure 4(d). The red line marks the vortex sheet consisting of the primary ring and shear layer, while the blue line indicates the evolution and distortion of the piston vortex. This pulsing of the vortex ring would indicate that the streamline topology should show an unsteadiness and a mechanism for detrainment. A recent computational

paper by Nitsche (2001) suggests that the shedding of vorticity into the wake of the ring is related to the variational principle of Lord Kelvin which for axi-symmetric rings means that the kinetic energy is at a local maximum, with respect to perturbations that preserve the circulation and impulse of the ring. Computational studies, e.g. Rom-Kedar *et al*. (1990) and Pozrikidis (1986), have shown how a perturbation to a vortex ring that is represented as an idealized symmetric vorticity distribution can result in unsteady entrainment and detrainment.

One obvious question that arise from these flow visualization results is what is the effect of varying the location where the piston motion is terminated, and at what S/D does the piston vortex/vortex ring interaction cease, where S is the distance the piston ceases its motion from the tube orifice, see figure 1(a). Flow visualization experiments for L/D=2.0 and Re_Γ=6530 revealed that any cessation of motion of the piston inside the tube reduces the amount of dye entrained from the piston vortex into the primary ring. The case for S/D~0.3 appeared to be the limit. When the piston ceases its motion inside the tube for S/D>0.3 there is no ingestion of any dye from the piston vortex.

5. Global Effects

A strong interaction of the piston vortex with the primary ring may alter the primary ring vortex trajectory, compared to the case where the piston motion is stopped inside the tube. Vortex trajectories were therefore measured for the case of L/D= 2 and Re_Γ=6530. The Reynolds number was selected to enable a comparison with the data sets of Didden (1979) and Weigand & Gharib (1997). The piston was stopped flush with the wall, or 2D

inside the tube. Measurements were made of the position of the core of the primary vortex, (Z_Γ, R_Γ), as defined in figure 1, using dye visualization.

5.1 Transient development and ring contraction.

The initial phase of the ring development is defined as while the piston is in motion. Results for the trajectory of the vortex core during this period, and shortly after the motion ceases are shown in figures 8 and 9.

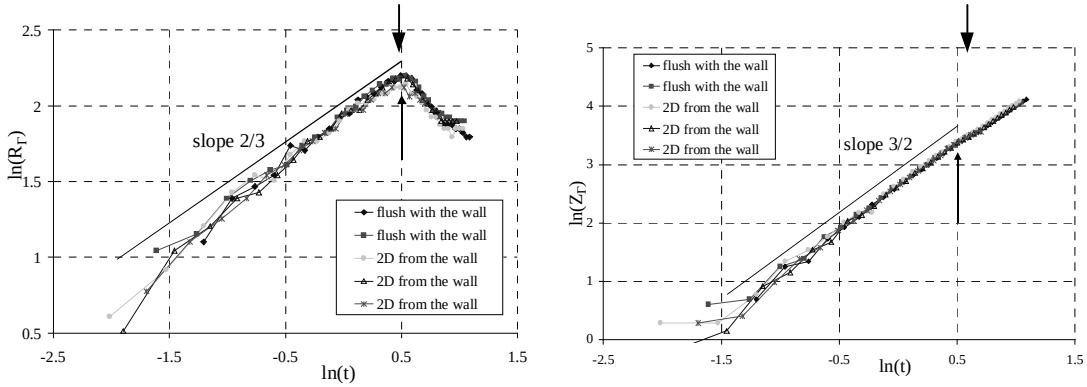

Figure 5 Variation of the primary ring core location, R_Γ and Z_Γ, with respect to time for Re_Γ=6530.

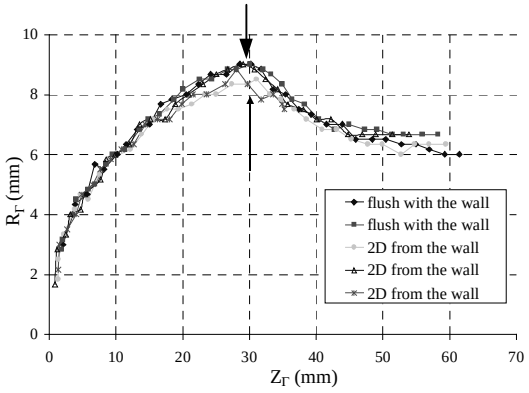

Figure 6 Trajectory of primary ring core for Re_Γ=6530.

The distinguishing aspect of these plots is that the trajectories are essentially identical. The data set for the R_Γ coordinate shows a $t^{2/3}$ growth during the development phase, whereas the Z_Γ coordinate shows a considerably faster growth rate, typically $t^{3/2}$. These measurements of R_Γ and Z_Γ agree with those of Didden (1979) and Weigand & Gharib (1997). The time at which the piston is stopped, t^*=2.17, is identified by an arrows in figure 8 and 9. At this point the trajectory of the ring undergoes a rapid reduction in diameter, before convecting for a time with an approximately constant velocity. For a specific L/D Didden (1979) and Weigand & Gharib (1997) found an independence of core trajectory on piston velocity.

The interesting aspect of the data in figure 9 is the fact that the contraction is almost identical for the case when the piston is finished inside the tube, and hence a stopping vortex is formed and the case when the piston is finished flush and the piston vortex is ingested. The final ratio of vortex diameter D_0 to piston diameter is $D_0 / D = 1.23$ which is in agreement with the empirical formulation of Auerbach (1988). This result suggests that the effect of the stopping vortex, produced at the orifice corner when he piston motion ceases, has little effect on the core trajectory and hence diameter. It would also seem to indicate that the effect of the piston vortex is weak.

The contraction of the ring diameter is also a feature of the studies where a “nozzle” is used as the generation device, e.g. Didden (1979) and Weigand & Gharib (1997). In these experiments, for L/D=2, gives a final vortex diameter of $D_{vortex} / D = 1.32$. The differing diameters for these two production devices can be also see in the computational data of James & Madnia (1996). Note that this difference exists for the ring characteristics produced at a tube and orifice for the same piston speed and stroke length.

Aurebach(1991) in a series of careful measurements notes that 60% ejected and 40% entrained for an orifice and 80% ejected and 20% entrained for a tube.

Current literature appearing on vortex rings has focused on the ring invariants, strength Γ, impulse I and kinetic energy T and the way these invariants are delivered by the generation apparatus. Classification of the ring from its invariants stems from the work of Norbury (1973) who solved for a class of vortex rings that were characterized by a vorticity distribution that was proportional to the distance from the axis of symmetry, $\omega = \Omega r$. Norbury rings are classified by a parameter α that represents the ratio of the area of the vortex to a length scale of the vortex. The range of α from $0 \rightarrow \sqrt{2}$ represent a rings of small cross section to Hill's spherical vortex. Each α yields a unique ring and associated invariants. These rings are somewhat idealized in that the vorticity distributions in experimental rings tend to be more Gaussian but provide a useful framework in which to consider the behavior of experimentally produced rings. The results of Norbury (1973) would seem to imply that the role of the image system and stopping vortex is not important in effecting the final diameter as it is defined by the invariants of production. It would also suggest that the rings produced at an orifice and nozzle, with the same L/D and velocity characteristic, are different as a result of how the apparatus delivers the invariants. Rosenfeld *et al* (1998) for example mention that the circulation of a ring produced at an orifice and nozzle can differ by as much as 5% and the suggested reason was a difference in vorticity cancellation. The computations of James & Madnia (1996) show a significant difference in the total impulse of the flow field for a ring produced at a nozzle and orifice. Unfortunately they do not calculate the impulse of the vortex alone for comparison. Variations in the way the impulse is

delivered to the rings for different geometries may be explained by considering the self-similar computations of Pullin (1978). In these 2D calculations of the starting flow past a 90^0 wedge and a flat plate a clear difference exists in the location of the vortex core, for a given strength, and hence it can be inferred that there will be a difference in impulse. This is a direct result of the flow geometry and system of images used for both calculations. Hence in conclusion it is suggested that the ring contraction is not a direct result of the system of images and stopping vortex but rather the ring relaxing to its natural state which is a function of its invariants. The generation geometry appears to be important in terms of determining how these invariants are produced.

5.2 Piston vortex leapfrogging

Figure 7 (a) shows the Z_Γ coordinate of the ring for larger values of t^* for L/D=2, Re_Γ=6530, and the two stopping geometries being considered, S/D=0 and 2. When the piston vortex is ingested, the velocity of the primary core slows at t^*~4.2. This correlates to a deceleration of the ring and occurs as the piston vortex is being convected through the ring, as shown in figure 2(b), t*=3.3. The data shown for S/D=2 display no such deceleration and the velocity of the ring appears to be almost constant. To more clearly illustrate the effect of the piston vortex as it orbits the primary ring, the mean Z_Γ core location was subtracted from the data sets. The results of this transformation are shown in figure 7(b). The mean location was based on the linear fit to the S/D=2 data set in figure 7(a).

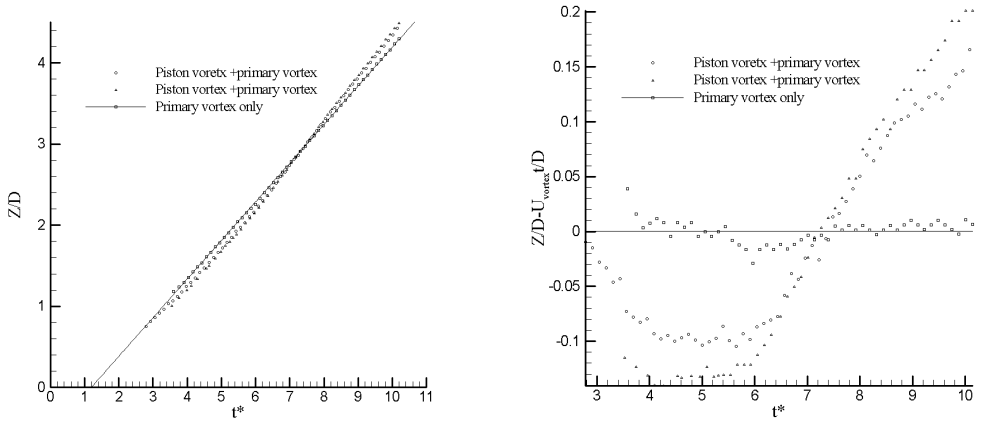

(a) (b)

Figure 7. Vortex core trajectories for Re_Γ=6530, L/D=2

These results indicate the presence of a vorticity distribution of the form sketched in figure 8. This distribution would act initially to decelerate the primary ring while the piston vortex accelerates through the core in a form similar to vortex leapfrogging, e.g. Yamada & Matsui (1978). As the piston vortex is comparatively weak compared to the primary ring, the induced effect of the piston vortex and hence the deceleration of the ring is weak, while the induced effect of the ring on the piston vortex is strong.

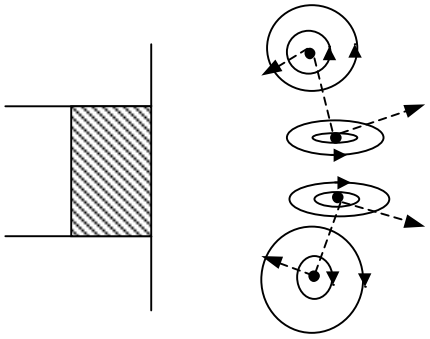

Figure 8. Leapfrogging and mutual induction effects of the primary ring and the piston vortex resulting in a deceleration of the main ring.

The plots in figure 7 (a) and (b) would also seem to indicate that at t^*~10 for identical Re_Γ there is a clear difference in the convection speed. To clarify this, the time at which the primary core reached Z/D=7.3 for L/D=2 and Re_Γ= 6530 was measured, and was found to be $t^*=15.1\pm0.1$ for the piston finishing flush with the wall and $t^*=16.4\pm0.1$ for the case when the piston finished 2D inside the tube. The ring diameters were equal in both cases. Therefore the distance traveled by the rings for a given interval is different, indicating a difference in ring strength, which is a direct consequence of ingestion of the piston vortex. To check this the location of the vortex core was measured for Re_Γ=10030, L/D=3, and S/D=0 and 1. The data showed a significantly different terminal speed. The time to reach Z/D=5.02 for the S/D=0 case was $t^*=11.3\pm0.1$ and for S/D=1, $t^*=12.3\pm0.1$. The conclusion that the rings have differing strength and that a form of leapfrogging is occurring is confirmed with the PIV measurements, section 6.

The major source of error in these measurements is not the location of the ring core, but cycle to cycle variations, caused by residual motions in the tank. For these experiments, the tank was allowed to settle for about 30 minutes between runs. If the settling time was not sufficient, misalignment of the rings occurred during ingestion, producing axisymmetric leapfrogging.

6. Topology of piston vortex/vortex ring interaction.

PIV experiments were performed to generate quantitative velocity and vorticity information during the development phase. The data acquisition system consisted of an argon ion laser, an externally triggered Cohu 6600-3000 series full frame transfer video camera, 659 x 496 pixels, with 10 bit resolution, a General Scanning 6120DT series oscillating mirror and an Epix frame grabber. Details of the PIV system hardware and

software, that are capable of producing at time difference between image of the order 0.5ms are contained in Allen & Smits (2001) and Allen *et al.* (2000).

Figure 9 shows a sequence of streamline patterns for the case when the piston finishes flush with the wall and inside the tube with application of a bias velocity equal to the speed of the piston.

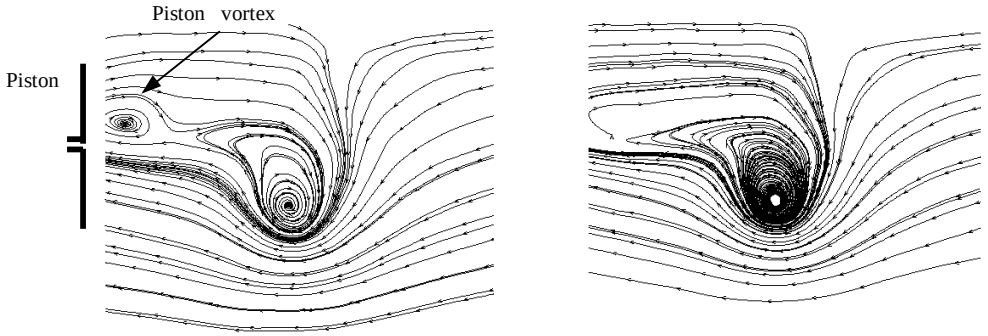

(a)

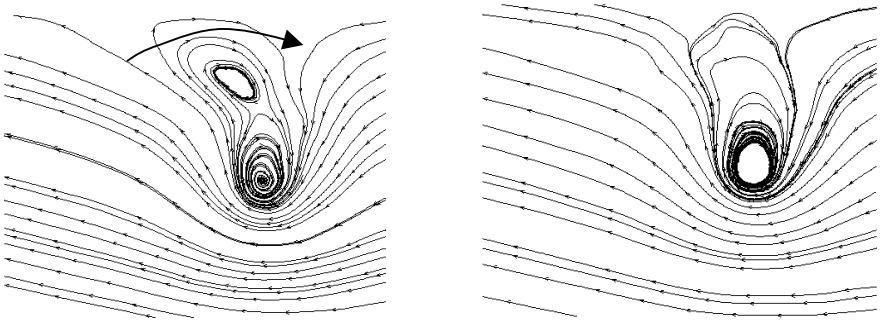

(b)

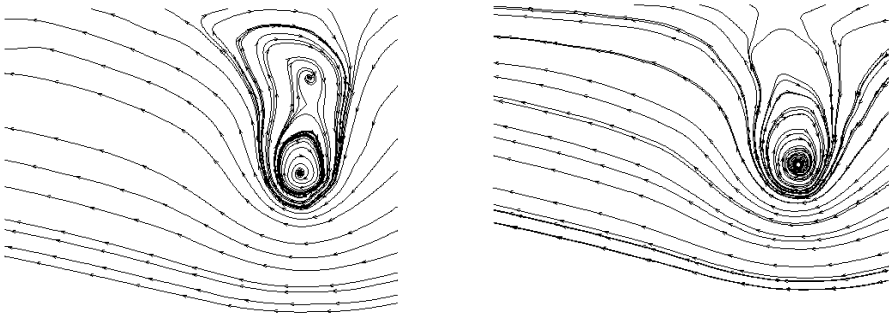

(c)

Figure 9 Streamline patterns for Re_Γ=6530, L/D=2, left column S/D=0, right column S/D=2 (a) t*=2.17 (b) t*=2.77 (c) t*=3.37

From these streamline pattern the presence of the piston vortex is clearly evident. The piston vortex can be seen convecting through the primary vortex as in the dye visualizations. Vorticity fields were generated from the velocity data sets using a global spline technique, as outlined in Spedding & Rignot (1993). Figure 10 shows a sequence of the developing vorticity fields when the piston finishes flush with the tube exit. Non-dimensional vorticity is defined as $\omega = \Omega U_P / D$ and the contours of ω in these vorticity contours in these plots are separated by three non-dimensional units.

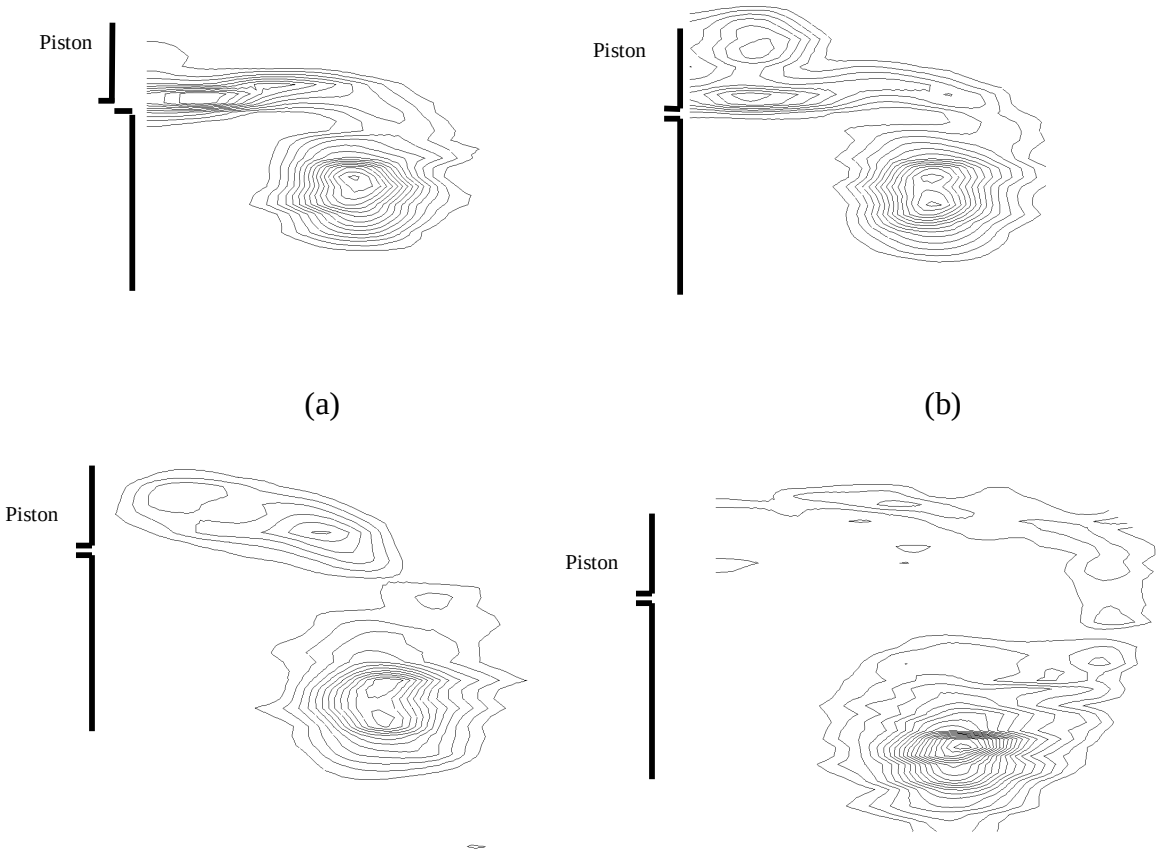

Figure 10 Vorticity fields for Re_Γ=6530 L/D=2, S/D=0 (a) t*=1.9(b) t*=2.17 (c) t*=2.77 (d) t*=4.0

Figure 10(a) shows the development of the primary ring while the piston vortex is still located inside the cylinder and the piston is still in motion. In figure 10(b) the presence of the piston vortex can be clearly seen emerging from the cylinder. This vorticity distribution appears very similar in form to the dye streakline image shown in figure 3(b). In figures 10(c) and (d) the piston has stopped and the piston vortex appears to be convecting toward the axis of symmetry and stretching along this axis toward the stagnation point of the primary vortex. This result also agrees well with the flow visualization that showed a bulge produced by the ingestion of the piston vortex, figure 2(b). These results also appear similar to that of Fabris & Liepmann (1997), who examined the late stages of ring development and who also comment that although there may be some cancellation of the vorticity from the shear layers across the axis of the ring, a significant amount of vorticity advects through the center of the ring and collects in the region of the forward stagnation point, resulting in a more complex vorticity distribution than may otherwise have been expected. The peak level of the non-dimensional vorticity in the primary vortex is ω~50 and the level in the piston vortex is ω~13, which agrees well with the results of Weigand & Gharib (1997) and Allen & Chong (2000). The vorticity distributions do not reveal any significant vorticity deposition into the wake.

A quantity of interest to describe the behaviour of vortex rings is the strength $\Gamma = \iint \Omega(r,\theta) dA$ and impulse $I = \rho\pi \iint \Omega(r,\theta) r^2 dA$. These quantities can be found evaluating an area integral over the vorticity fields. Figure 11(a) and (b) show Γ / υ and

$I/(\rho\pi D^2/4U_0)$ versus t^* for the case where the piston finishes flush with the wall, and when it finished 2D inside the tube for Re_Γ=6530.

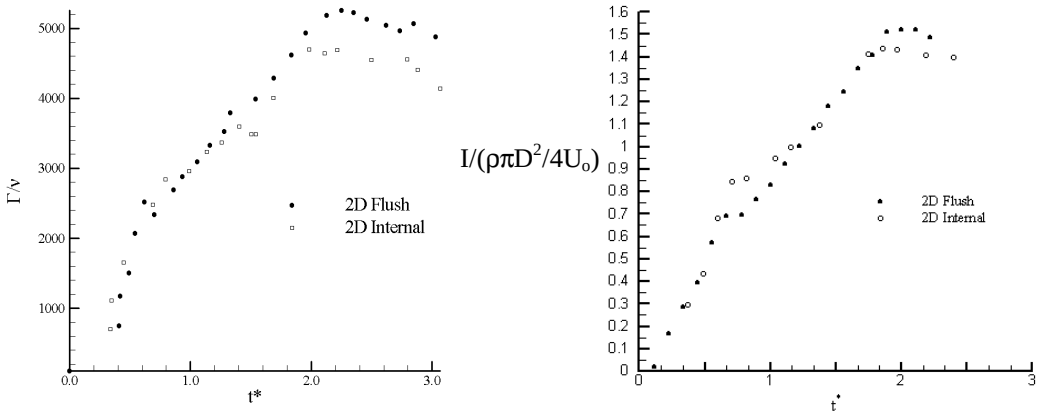

(a) (b)

Figure 11 (a) Γ/ν and $I/(\rho\pi D^2/4U_0)$ versus t^* for Re_Γ=6530 and S/D=0,2 L/D=2

The results show that when the piston finishes flush with the wall the ring has a larger larger impulse and strength. This coroborates the conclusion made in setion 5.2 where it was conjectured that the increased convection speed for S/D=0 was related to higher circulation of the primary ring. The size of the difference in ring strength, of the order 6%, is similar to the difference in convection speed. This difference in strength and impulse is most clearly illustrated in figure 12 which shows the vorticity distributions at the instant the piston motion has ceased for S/D=0 and S/D=2. The larger integral, and hence strength and impulse , for the S/D=0 case is clearly due to the presence of the piston vortex that can be seen being ejected in front of the piston. The results for ring strength, for an L/D=2, are of the order $\pm 5\%$ to that shown in Didden (1979), figure 15. It should also be noted that the area integral used for the calculation of impulse and strength for the case where the piston ceases its motion inside the tube does not

incorporate the stopping vortex and hence the impulse and strength calculated are for the primary ring. With our two stopping configurations, the small variation in impulse and strength is clearly explained as a result of the ingestion of the piston vortex, rather than an effect of the stopping vortex.

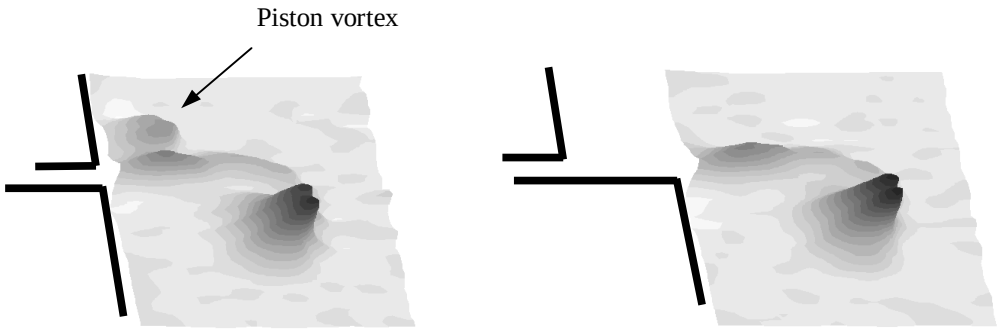

Figure12 Variation in vorticity distribution at Re_Γ=6530, t*=2.17 for (a)S/D=0 (b) S/D=2

7. Development of azimuthal instabilities on the piston vortex.

Glezer (1988) noted the presence of an azimuthal core instability on the primary ring that consisted of vortex tubes, alternating in sense, wrapped around the main core of the vortex that resembled the braids that appear in shear layers , e.g. Bernal and Roshko (1986). He also commented that these tubes are responsible for the entrainment and detrainment of fluid to the and from the vortex ring and suggested that these tubes had the their origin on the connecting shear layer between the vortex core and the orifice and that their presence accelerates the transition to turbulence.

To determine the origin of these instabilities on the ring observed by Glezer and commented on by Auerbach (1991), a global visualization technique was employed. A metallic precipitate was created at the edge of the orifice using a loop of tinned solder. The thickness of the solder loop was of the order 0.5*mm* and was located on the wall a

distance of 1*mm* from the orifice to as to not disturbed the vortex ring generation process. The solder, acting as the anode, connected to an 80V power source. The primary benefit of this method is that white light could be used to provide a three dimensional image of the ring development. The Schmidt number of the precipitate is of order 1000, see Taneda (1977) for details. Figure 13 shows a sequence of results for the case when piston motion finishes flush with the wall.

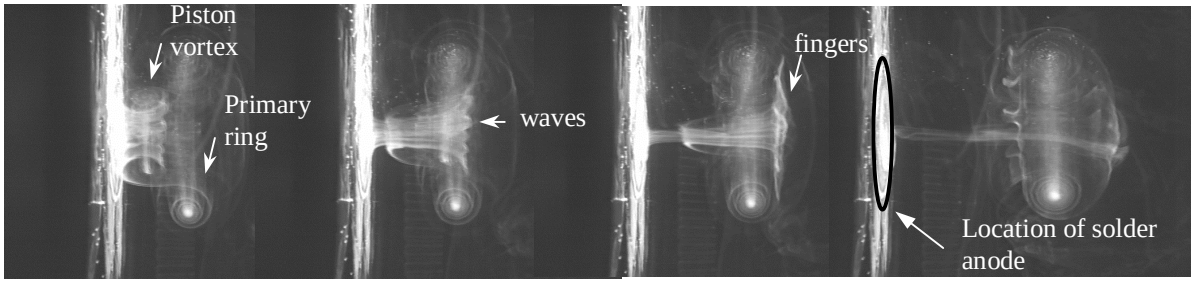

(a) (b) (c) (d)

Figure 13 Precipitate flow visualization images for Re_Γ=6530 L/D=2 (a) t*=2.17 (b) t*=2.65 (c) t*=3.3 (d) t*=5.8

Figure 13(a) shows the piston vortex and primary ring at the instant the piston motion has stopped. Wave like structures are seen on the outer turn of the piston vortex. No waves are apparent on the core of the piston vortex, or on the primary ring. These wave-like structures persist throughout the entrainment process. In figure 13(b) the waves on the piston can be seen passing through the primary ring. As the piston vortex reaches the stagnation point of the main ring, these structures can be seen wrapping rapidly around the outside of the primary vortex in a finger-like fashion, figure 13(c). In figure 13(d), the tips of the structures can be seen in the wake of the ring as a series of jellyfish-like tentacles. To gain a further insight into the nature of these structures, their time evolution and wavelength, laser cross sections were taken through planes perpendicular to the

direction of propagation of the ring. Results of flow visualization experiments using fluorescent dye are shown in figure 14 for a range of Z/D locations from the wall, where Z is the streamwise distance from the orifice exit.

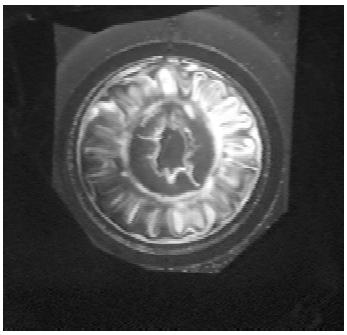

(a) Z/D= -1.64 t*=3.32

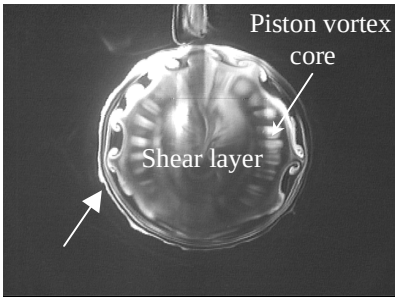

(b) Z/D = 0.35 t*=4.24

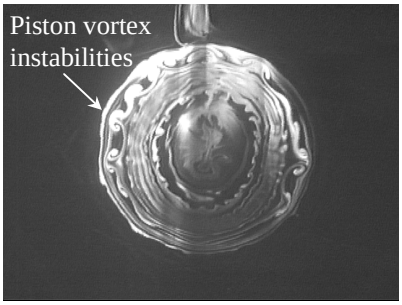

(c) Z/D=0.35 t*=4.32

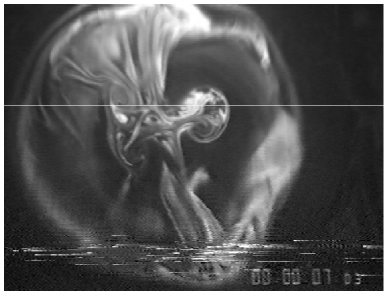

(d) Z/D=3.15 t*=6.85

Figure 14 Laser cross sections for Re_Γ=13390 and L/D=4, S/D=0

Figure 14(a) shows a cross section of the piston vortex at the location, Z/D= -1.64, t*=3.32. This represents a cross-section inside the tube, before the piston vortex has been ejected. Periodic structures can be seen distributed around the azimuth on the piston vortex, indicating that the source of the instability is not related to the presence of the primary ring. Figures 14(b) and (c) show cross-sections at a location Z/D=0.35, downstream of orifice. The cross sections marked A and B in figure 2(a) and (b) mark the approximate location where these cross sections are taken relative to the evolution of the piston vortex. In the images in figure 14(b) and (c) the primary ring has already passed through the laser sheet. The outer circle of dye represents the shear layer that connects the primary ring to the orifice exit. Figure 14(b) shows the head of the piston vortex as it starts to enter the illumination plane. Instabilities on the outer edge of the piston vortex can be clearly seen, as can the connecting filaments running across the top of the piston vortex. Figure 14(c) shows the same cross section through the core of the piston vortex a short time later. The connecting filaments are no longer visible, but instabilities on the outer edge of the piston vortex can be clearly seen, along with some waviness on the inner turns of the piston vortex. The visualizations indicate the presence of vorticity filaments aligned in a plane perpendicular to the azimuthal direction. This represents a significant reorientation of the vorticity on the piston vortex. The number of azimuthal structures is of order twelve. Varying Re_Γ did not appear to significantly alter the number of waves that were forming but did effect how rapidly they developed. The instability does not seem to have its origin on the piston vortex core. Figure 14 (d) shows a cross section through the vortex at a location Z/D=3.15, t*=6.85. The cross section is shown as C in figure 2(c) represents the approximate location of this point. This image shows the

"bulge" identified in earlier visualizations. The presence of streamwise piston-generated fingers can be seen clustered in the stagnation point region. The stretching of two of these structures around the outer periphery of the primary vortex is also evident.

8 Instability mechanism

It appears from the flow visualization images that the instability has its source on the outer turn of the piston vortex. In order to construct a physical mechanism for the generation of these structures one must consider how the piston vortex is being generated. Figure 15 shows an example of the streamline pattern and vorticity field in the region of the junction of the piston/cylinder wall from Allen & Chong (2000). This is a cross-section of one side of the piston vortex relative to an observer moving with the piston.

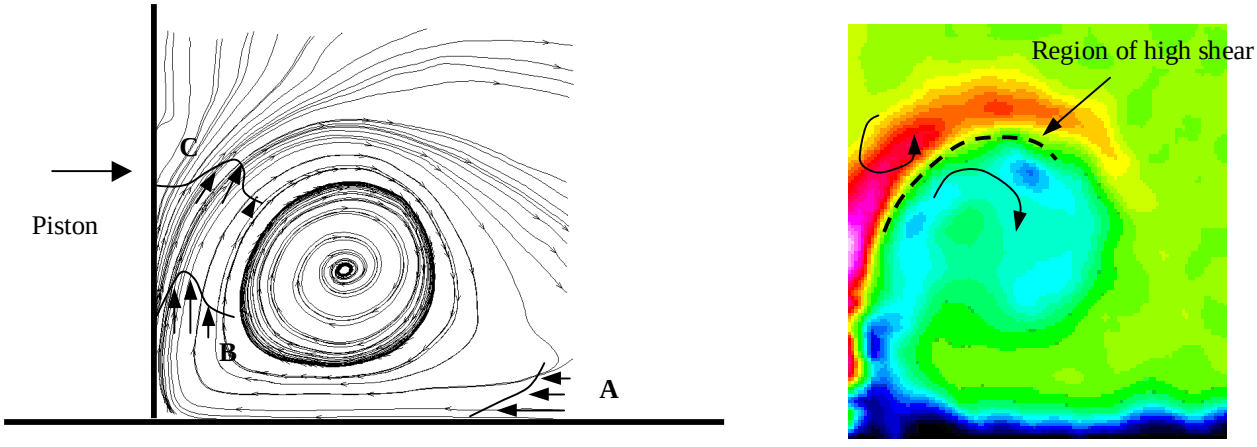

Figure 15 Streamline pattern (a) and vorticity field (b) from Allen & Chong (2000)

The process of formation of this structure is that when the piston is set in motion, a boundary layer forms on the cylinder wall, shown with the velocity profile at **A**. The boundary layer is turned through 90^{o} at the piston junction resulting in the production of

significant secondary vorticity on the piston face and resulting in a “wall jet” type velocity profile, shown at **B**. The boundary layer then diverges rapidly away from the piston surface, shown by the velocity profile at point **C** and rolls into a vortical structure, described in this paper as the “piston vortex”. The wall jet nature of the velocity profile on the piston face indicates two regions of opposite signed vorticity, and diverging flow at point **C** is subject to high curvature. These two layers of opposite signed vorticity can be clearly seen in figure 15(b). A wall jet subject to concave curvature is unstable due to the presence of centrifugal forces, see Floryan & Saric (1984). It is in the inner flow, the section of the flow between the wall and the point of maximum velocity, that the instability will first develop in a wall jet subject to concave curvature. The control parameter for the stability of wall jets subject to concave curvature is the Görtler number, $Go = U_\infty \delta / \upsilon \times \sqrt{\delta / R}$, where U_∞ is the maximum velocity of the wall jet, R is the radius of curvature and δ is the wall jet thickness. A criteria for the development of Görtler vortices in the wall jet with concave curvature is $Go > 1.0$. There is no critical wavenumber and the characteristics of the vortices are determined by the disturbance growth process. Experiments to determine the natural wavelength of Görtler vortices have been found to be extremely sensitive to the properties of the apparatus and its flowfield, see Tani & Sakagima (1964). Bippes(1978) recorded the wavelength of the Görtler as being that of the highest amplification rate from linear theory and once the wavelength is established it is preserved downstream. From Floryan (1987) if we consider the dimensionless wavelength parameter $\Lambda = F^{1/3} \lambda^{1/3} \upsilon^{-1} (\lambda / R)^{1/2}$. Where F is the dimensional “flux of external momentum flux”, see Glauert (1956). Λ is constant in the flow direction in order to follow a vortex of constant dimensional wavelength λ. The

curve of maximum growth from the linear stability analysis of Floryan (1987) shows a variation of Λ from 48 to 85. From experiments with the piston moving at 66mm/sec an estimate of $U_\infty \approx 30$mm/sec. An approximation for the wall jet thickness in is $\delta \approx 8mm$ and radius of curvature of $R \approx$ 12mm.

This results in a Görtler number, $G_o = U_\infty \delta / \upsilon \sqrt{\delta / R}$, in excess of one hundred and hence instabilities should be present. Using a crude approximation for the velocity profile an estimate can be made for $F \approx 1.63 \times 10^5 \text{mm}^7\text{sec}^{-3}$ which results in an approximation for $\lambda \approx 1.4mm$ to $8mm$. The wavelength of the structures in figure 14(a) is of order eight millimeters and hence it would appear that the instability is of centrifugal form. Once the region of secondary vorticity plume and neighboring piston vortex has been perturbed it is anticipated that the non-linear growth of the instability follows a similar non-linear growth mechanism outlined by Lasheras *et al.* (1986). They presented a physical model for the generation of the streamwise structures via non-linear vortex stretching and tilting in the highly strained braid region of a shear layer. A similar region of high shear exists on the outer turn of the piston vortex, as illustrated in figure 15(b) This stretching process is illustrated in figure 16(a). This instability is rolled/entrained into the piston vortex as the structure develops in front of the advancing piston.. When the piston vortex is ejected and ingested into the primary ring the instabilities produce the fingers seen in figure 13(c) and the filaments in figure 14(a). This development process is shown in schematic form in figure 16(b), where the rolled up vortex sheet that constitutes the primary ring is shown as being connected to the piston vortex and the instability is superimposed on the vortex sheet that is wrapped around the primary ring. In this image blue represents dye from the piston vortex and red represents the primary ring.

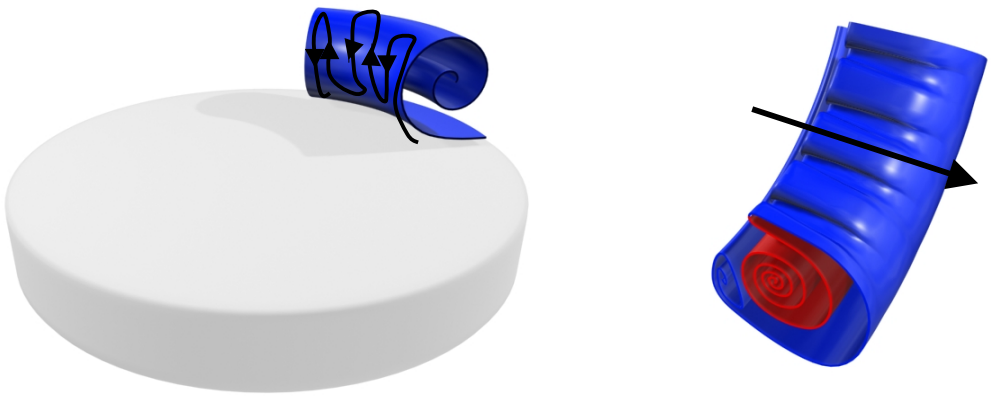

Figure 16(a) Schematic of instability development on piston and (b) ingestion of piston vortex and instability during steady translation

8. Transition to turbulence

If Re_D exceeds six hundred, then as the vortex convects away from the tube, azimuthal waves associated with the Tsai-Widnall instability begin to appear. This leads to an eventual breakdown to turbulence. These waves develop because the strain field at a perturbed point on the vortex ring is sufficient to overcome the self-induced azimuthal core rotation. The most unstable waves grow at an angle of the order 45^o to the axis of symmetry, without precessing about the ring core. The image in figure 17(a) shows the formation of these waves for Re_Γ=6530 at Z/D~8. Saffman (1978) noted that although the mechanism for the generation of waves on the ring is an inviscid one, the number of waves that appear on a vortex ring is a function of the shape of the vorticity distribution within the ring, and hence a function of Reynolds number. The calculations of Saffman (1978) agree well with the experiments of Leiss & Didden (1978), who found an experimental variation of the number of waves forming on the ring from $4 \rightarrow 11$ as Re_D was varied from $2{,}000 \rightarrow 10{,}000$ with L/D=1.4. In the current experiments it was found

that the number of waves forming on the primary ring appears to be insensitive to whether the piston vortex is ingested or not for a given Re_Γ. For Re_Γ=6530 the number of waves is of the order six. The image in figure 17(b), which shows the classical Tsai-Widnall instability just prior to vortex breakdown to turbulence, also shows evidence of filaments on the outer diameter. These structures had their origin on the piston vortex.

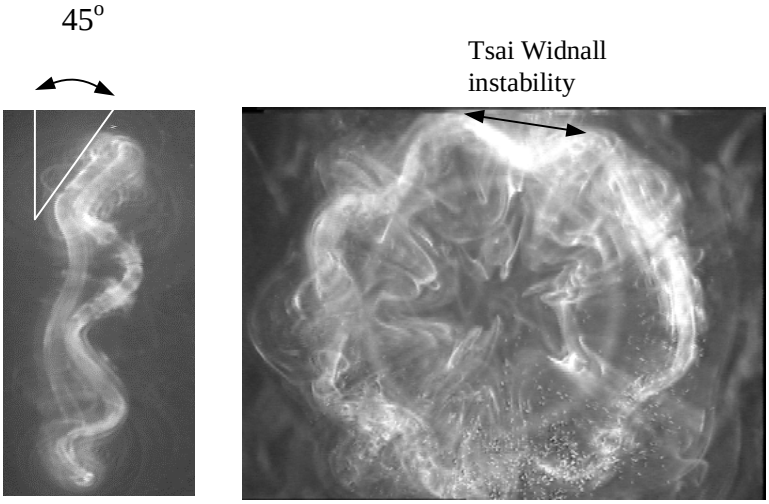

Figure 17 Development of Tsai-Widnall instabilities Re_Γ=6530, t*= 17, S/D=0, L/D=2,

The distance to transition to turbulence, as determined from flow visualization experiments, are shown in figure 18. The results show there is an effect of the piston vortex on the transition distance. Although the piston vortex does not appear to affect the number of waves appearing on the ring, it appears to have a secondary effect in terms of amplifying the growth of the Tsai-Widnall instability and hence reducing the distance of translation before breakdown to turbulence occurs. Comparison with the data of Leiss &

Didden (1978) was good for the case of L/D=1.4 and the piston finishing inside the tube and the results suggest that the transition map of Glezer(1988) needs re-evaluation. The error in measurements of distance to transition is of the order $\pm 4\%$

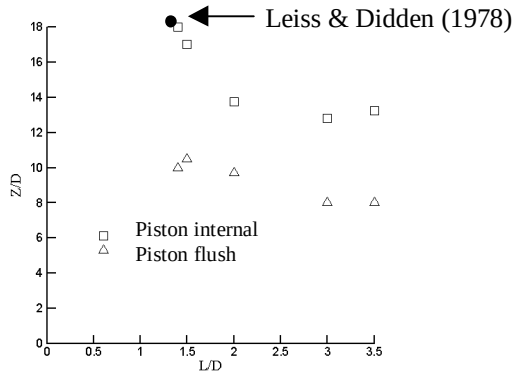

Figure 18. Distance traveled from tube exit to turbulence breakdown for Re_D=3120

9. Conclusions

The simple formation geometry of a piston finishing flush with a normal wall to produce a vortex is shown to introduce an interesting flow complexity. While eliminating the stopping vortex, a piston vortex is ejected and entrained into the primary ring. The L/D in this experiment was varied from $1 \rightarrow 4$, where L is the stroke of the piston. In all the cases when the piston was finished flush with the wall, ingestion occurred. This ingestion appears to have a measurable effect on the speed of the primary ring and measurements confirm that ingestion of the piston vortex provides an added impulse to the ring. The absorption of the piston vortex has also been measured in terms of its effect on the unsteady streamline field and vorticity distribution. The piston vortex appears to be entrained toward the forward stagnation point on the ring, where it is rapidly strained and convected around the periphery of the primary vortex core. There is evidence of a centrifugal instability on the piston vortex which has the effect of generating vorticity

filaments in the plane perpendicular to the azimuthal direction. These instabilities are entrained into the main ring and could be the origin of the instabilities observed by Glezer (1988). It appears that the piston vortex, although not affecting the basic mechanism for transition, has a secondary effect on transition in that it reduces the distance the ring convects before transition occurs because it amplifies the growth rate of the Tsai-Widnall instability. This would also suggest that the transition map proposed by Glezer (1988) is geometry specific.

The authors would like to acknowledge the support of Professor A.J. Smits and the NSF, grant number CTS-9706902

REFERENCES

ALLEN, J.J. & CHONG, M.S. 2000 Vortex formation in front of a piston moving through a cylinder, *J.Fluid Mech,* **416,** 1-28.

ALLEN, J.J. & SMITS, A.J. 2001 Energy harvesting eel. *Journal of Fluids and Structures,* **15,** 629-640

ALLEN, J.J., AUVITY, B. & SMITS, A.J. 2000 Interaction of a vortex ring with a piston vortex. 9th International Symposium on Flow Visualization. Edinburgh, August 22-25. ISBN 0 9533991 17

AUERBACH, D. 1987 Experiments on the trajectory and circulation of the starting vortex, *J.Fluid Mech.* **183**, 185-198.

AUERBACH, D. 1991 Stirring properties of vortex rings. *Phys. of Fluid* **A 3 (5)** , 1351

BERNAL, L.P. & ROSHKO, A. 1986 Streamwise vortex structure in plane mixing layers *J. Fluid Mech.* **170**, 499-526

BIPPES, H. 1972 NASA TM-72243

CATER, J., SORIA, J. & LIM, T.T. 1998 Vortex ring formation at an orifice. ETC7.

DIDDEN, N. 1979 On the formation of vortex rings rolling-up and production of circulation, *Z.Angew. Math. Phys.* **30**, 101-116.

FLORYAN, J.M. & SARIC, W.S. 1984 Wavelength selection and growth of Görtler vortices. *AIAA Journal* **22** , 1529-1538

FLORYAN, J.M. 1987 Görtler Instability of wall jets. *AIAA Journal* **27**, 112-115

FABRIS, D. & LIEPMANN, D. 1997 Vortex ring structure at late stages of formation. *Phys. Fluids.* **9**, 2801-2803

GHARIB, M., RAMBOD, E. & SHARIFF, K. 1998 A universal time scale for vortex ring formation, *J. Fluid Mech.* **360**, 121-140.

GLAUERT,M.B. 1956 The wall jet. *J.Fluid Mech.* **1**,625

GLEZER, A. 1988 The formation of vortex rings, *Physics of Fluid.* **32**, 3532-3542.

GLEZER, A. & COLES, D. 1990 An experimental study of a turbulent vortex ring. *J.Fluid Mech.* **211**, 243-283.

HEEG, R.S. & RILEY, N. 1997 Simulations of the formation of an axisymetric vortex ring, *J.Fluid Mech.* **339**, 199-211.

HUGHES, M.D. & GERRARD, J.H. 1971 The stability of unsteady axisymmetric incompressible pipe flow close to a piston. Part 2. Experimental investigation and comparison with computation, *J. Fluid Mech.* **50**, 645-655.

JAMES, S. & MADNIA, C.K. 1996 Direct numerical simulation of a laminar vortex ring. *Phys. of Fluids* **8**, 2400-2414.

KADEN, H. 1931 *Ing. Arch.* **2**, 140-168.

LASHERAS, C., CHO, J.S. & MAXWORTHY, T. 1986 On the origin and evolution of streamwise vortical structures in a plane, free shear layer. *J.Fluid Mech.* **172**, 231-258

LEISS, C. & DIDDEN, N. 1978 *ZAMM* **56**, T206.

LIM, T.T. & NICKELS, T.B 1995 Vortex rings. *Vortices in Fluid Flows* ed. Green, S.I., Kluwer.

LIM, T.T. 1997 On the role of Kelvin-Helmholtz like instability in the formation of turbulent vortex rings, *Fluid Dynamics Research*. **21**, 47-56.

LIM, T.T. 2000 A note on the generation of a vortex ring using Glezer's technique. Private communication. January 2000

MAXWORTHY, T. 1972 The structure and stability of vortex rings. *J. Fluid Mech.* **51**, 15-32.

MAXWORTHY, T. 1974 Turbulent vortex rings. *J. Fluid Mech.* **64**, 227-240.

NITSCHE, M. & KRASNY, R. 1994 A numerical study of vortex ring formation at the edge of a circular tube, *J.Fluid Mech*. **276**, 139-161.

NITSCHE, M. 1996 Scaling properties of vortex ring formation at a circular tube opening. *Phys. of Fluids* **8**, 1849-1855.

NITSCHE, M. 2001 Self-similar shedding of vortex rings. *J.Fluid Mech*. **435**, 397-407.

POZRIKIDIS, C. 1986 The nonlinear instability of Hill's vortex. *J.Fluid Mech*. **168**, 337-367.

PULLIN, D.I. 1978 The large-scale structure of unsteady self-similar rolled-up vortex sheets, *J.Fluid Mech.* **88(3)**, 401-430.

PULLIN, D.I. & PERRY, A.E. 1980 Some flow visualization experiments on the starting vortex, *J. Fluid Mech.* **97**, 239-255.

ROM-KEDAR,V., LEONARD, A. & WIGGINS, S. 1990 An analytical study of the transport, mixing and chaos in an unsteady vortical flow. *J.Fluid Mech.* **214** , 347-394.

ROSENFELD, M., RAMBOD, E. & GHARIB, M. 1999 Circulation and formation number of laminar vortex rings. *J.Fluid Mech.* **376** , 297-318.

SAFFMAN, P.G. 1978 The number of waves on unstable vortex rings, *J. Fluid Mech.* **84**, 625-639.

SHARIFF, K. & LEONARD, A. 1992 Vortex rings. *Ann. Rev. Fluids Mech.* **24** , 235-279.

SHEFFIELD, J.S. 1977 Trajectories of an ideal vortex pair near an orifice. *Phys. of Fluids* **20**, 543-545.

SPEDDING, G. & RIGNOT, E. 1993 Performance analysis and application of grid interpolation techniques for fluid flows. *Expt. Fluids* **10**, *417-430.*

TABACZYNSKI, R.J, HOULT, D.P. & KECK J.C. 1970 High Reynolds number flow in a moving corner, *J. Fluid Mech.* **42**, 249-255.

TANEDA, S. 1977. Visual study of unsteady separated flows around bodies. *Prog. Aerospace Sc.* , **17**, 287-348

TANI, I & SAKAGAMI, J. 1964 Boundary layer instability at subsonic speeds. *Proc. of third congress of the International Council of Aerospace Science*, Spartan, Washington, D.C 391-403

TAYLOR, G.I. 1960 *Aeronautics and Aeromechanics*. Pergamon.

WEIGAND, A., GHARIB, M. 1997 On the evolution of laminar vortex rings, *Exp. in Fluids*, **22**, 447-457.

WIDNALL, S.E. & TSAI, C.Y. 1977 The instability of the thin vortex ring of constant vorticity. Philos. Trans. R. Soc. London Series. A 287, 273-305.

YAMADA, H. & MATSUI, T. 1978 Preliminary study of mutual slip-through of a pair of vortices, *Phys. of Fluid.* **21**, 292.